Fatigue Life of Postbuckled Structures with Indentation Damage

Carlos G. Dávila[1]
NASA Langley Research Center, Structural Mechanics and Concepts Branch, Hampton, VA, 23681

Chiara Bisagni[2]
Delft University of Technology, Faculty of Aerospace Engineering, 2629HS Delft, The Netherlands

The fatigue life of composite stiffened panels with indentation damage was investigated experimentally using single stringer compression specimens. Indentation damage was induced on one of the two flanges of the stringer. The experiments were conducted using advanced instrumentation, including digital image correlation, passive thermography, and in-situ ultrasonic scanning. Specimens with initial indentation damage lengths of 37 mm to 56 mm were tested in fatigue and the effects of cyclic load amplitude and damage size were studied. A means of comparison of the damage propagation rates and collapse loads based on a stress intensity measure and the Paris law is proposed.

I. Introduction

Composite structures can sustain a high degree of deformation during impact without developing visible cracks, even though the internal substructure is damaged. Thus, the traditional reliance on visual detection to find damage, which worked well for metal skins that dent easily, is inadequate for composite airframes. Therefore, the design and certification of a composite airframe must rely upon a thorough understanding of the strength and life reductions caused by barely visible impact damage (BVID).

The single stringer compression (SSC) specimen was developed by the authors to study the response and the failure of a multi-stringer panel loaded in compression[1, 2]. The SSC specimen represents an intermediate level of complexity between coupon-level specimens and structural components while exhibiting most of the response characteristics of more complex multi-stringer panels. The experimental and numerical advantages of the SSC specimen are the low manufacturing and testing costs and the moderate computational model size requirements, respectively.

The SSC specimen is composed of a skin and a hat-shaped stringer that divides the specimen into two half bays; the dimensions are shown in Fig. 1. The skin consists of an 8-ply quasi-isotropic laminate with a stacking sequence of $[45°/90°/-45°/0°]_S$ and a total thickness of 1 mm. The stringer consists of a 7-ply laminate with a symmetric stacking sequence of [-45°/0°/45°/0°/45°/0°/-45°], which results in a total thickness of 0.875 mm. The skin and stringer are co-cured in an autoclave and the material is IM7/8552 prepreg tape.

The test results presented in this paper represent the fourth phase of experimental and analytical investigations to evaluate the effect of defects on the damage tolerance and fatigue life of SSC specimens[2-5]. The first phase of this testing effort, which was conducted in 2009, provided an initial indication of the effect of defect size on the collapse loads of SSC specimens. These test results were also used to validate a shell-based progressive damage finite element model. The second test campaign was performed in 2011 with additional instrumentation that included detailed ultrasonic testing (UT) of the specimens as well as the use of digital image correlation to measure the postbuckling deformations during the test. Fatigue tests were first conducted during the third test phase, which was conducted in 2013, and the instrumentation was expanded to include passive thermography and in-situ UT. The specimens in phases I and II were fabricated at the Politecnico di Milano in two different batches. The specimens for phases III and IV were made in one batch by a well-known aerospace manufacturer of composite structures.

[1]Aerospace Research Engineer, MS 190, Structural Mechanics and Concepts Branch, NASA LaRC, Hampton, VA, carlos.g.davila@nasa.gov, AIAA Member.
[2]Professor and Chairholder of Aerospace Structures and Computational Mechanics, Kluyverweg 1, 2629HS Delft, The Netherlands, C.Bisagni@tudelft.nl, AIAA Associate Fellow.

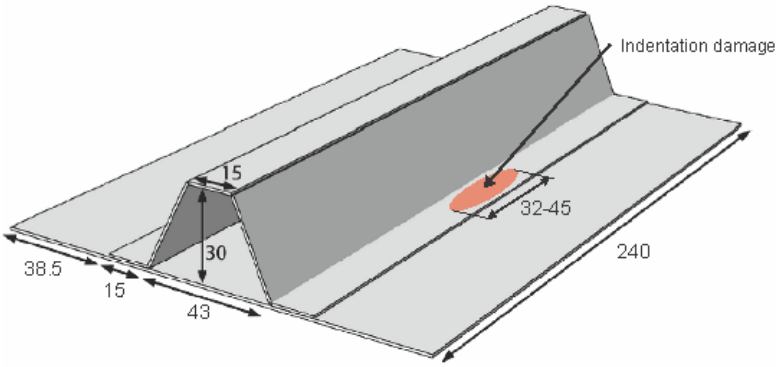

Figure 1. Nominal dimensions of the SSC specimen (in mm).

In contrast with the previous test campaigns, where initial bond defects were introduced by placing a Teflon film between the skin and one of the stringer flanges, the initial damage in the present test campaign (fourth test phase) was induced to the panel by quasi-static indentation. One specimen was subjected to quasi-static loads until collapse, and four specimens were subjected to cyclic loading. The collapse loads of all the specimens tested in phases I through IV are compared for the first time in this paper.

The remainder of this paper consists of the following sections. First, the procedure used for the indentation and the damage zones that were induced are described. Then, measurement of the initial shape of the skin is discussed and typical initial deformations and indentation depths are shown. The test equipment used, including the test frame and instrumentation used to monitor the propagation of fatigue damage is described in Section IV. The results of the quasi-static and fatigue tests are described in Sections V and VI, respectively. A comparison of the fatigue test results is presented in Section VII, and the collapse loads for all four test campaigns completed to date are compared in Section VIII.

II. Indentation Damage

In the present study, damage similar to BVID was induced on the skin side of the panel by quasi-static indentation. The advantages of indentation compared to impact include the simplicity of application, less dependence on boundary conditions, better controllability and repeatability of the imparted damage, and the ability to re-indent at the same location to increase the extent of damage. The hydraulic indenter used in this work is shown in Fig. 2. The radius of the hemispherical indenter is 12.7 mm.

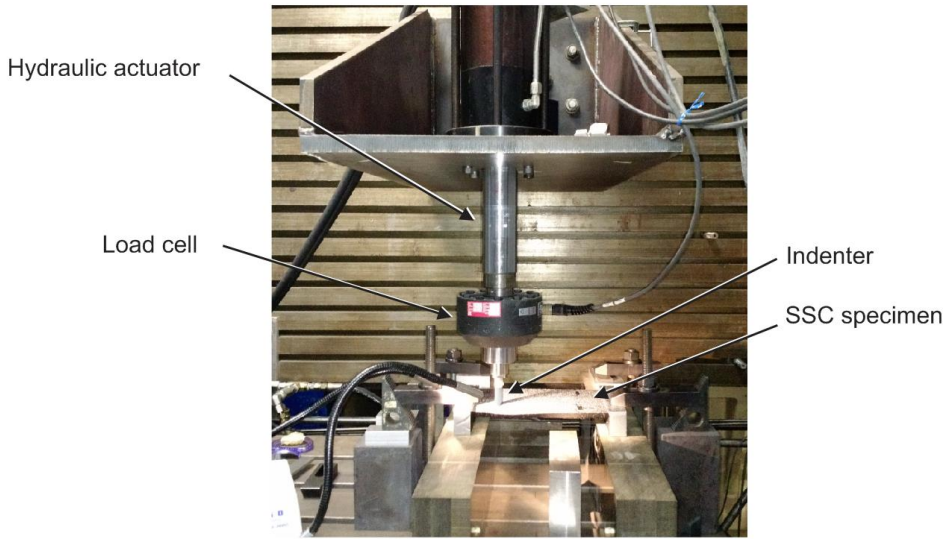

Figure 2. Hydraulic indenter used to induce initial damage onto the flange of the SSC specimen.

Five specimens, referred-to as SSCS-1 to -5, were tested. The specimens were indented on the skin side at the mid-span of the specimen, as illustrated in Fig. 1. Specimens SSCS-1 and SSCS-5 were indented under the flange termination (edge indent), and the three remaining specimens were indented at the center of the flange. Previous experience using Teflon films as crack initiators[4] indicate that when using rectangular 40-mm-long Teflon inserts, a cyclic load of approximately 80% of the collapse load results in fatigue lives of a few tens of thousands of cycles. With 20-mm Teflon inserts, the cyclic load required for any fatigue damage propagation was found to be too close to the collapse load to avoid fatigue runouts or unintended collapses. Therefore, a target indentation damage size of approximately 40 mm was selected.

To verify that the indentation load would not cause damage to areas other than under the indenter, a finite element model of the indentation process was constructed using Abaqus[6]. The model, shown in Fig. 3, indicates that at an applied indentation load of 1.28 kN, the predicted load for initiation of indentation damage, the strains do not exceed 4000 μstrain anywhere outside of the immediate area around the indenter. Strains below 10,000 μstrain are not expected to cause damage to the material.

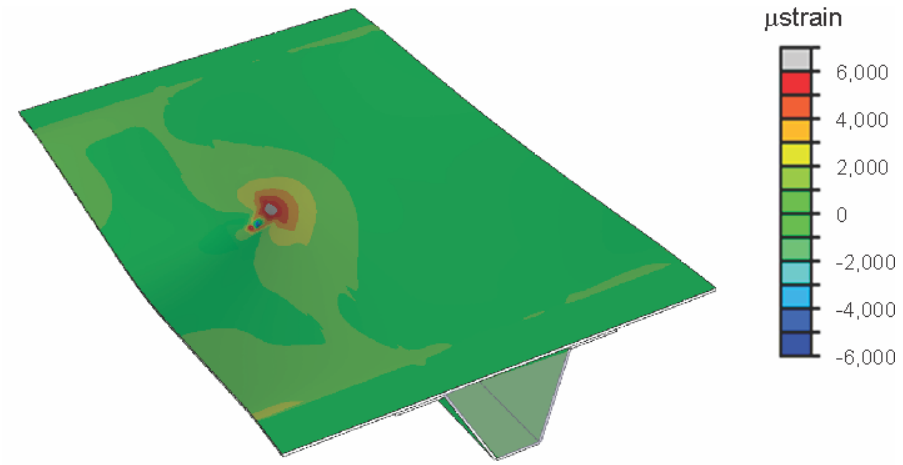

Figure 3. Strain plot for finite element damage model of indentation with an applied load of 1.28 kN.

To determine the indenter force/displacement required to obtain the desired damage size, a survey was conducted using undamaged portions of previously tested specimens. It was found that the size of the damage, measured along the length of the stringer flange, correlates well with the displacement of the indenter after the first load drop. This displacement of the indenter after damage initiation is referred to here as "drag". For the specimens in the current study, an indenter drag of 1.65 mm after the point of initiation induced approximately 45 mm of damage along the skin/stringer interface for the edge indentation, and 35 mm of damage for the center indentations. The load-displacement responses for all five specimens tested are shown in Fig. 4. It can be observed that the stiffness of the response for center indentations is considerably higher than that for edge indentations.

UT images of the induced indentation damage for the five specimens are shown in Fig. 5 with dimensions in mm. The 31-mm damage size initially obtained for specimen SSCS-3 was considered too small for fatigue testing, so it was subsequently re-indented. Upon re-indentation, the damage size extended to 56 mm.

It can be observed that the length of the damage is greater for edge indentation than it is for center indentation. It is also apparent that in all specimens the damage reaches the inside web/flange corner, especially in the case of the re-indentation of specimen SSCS-3.

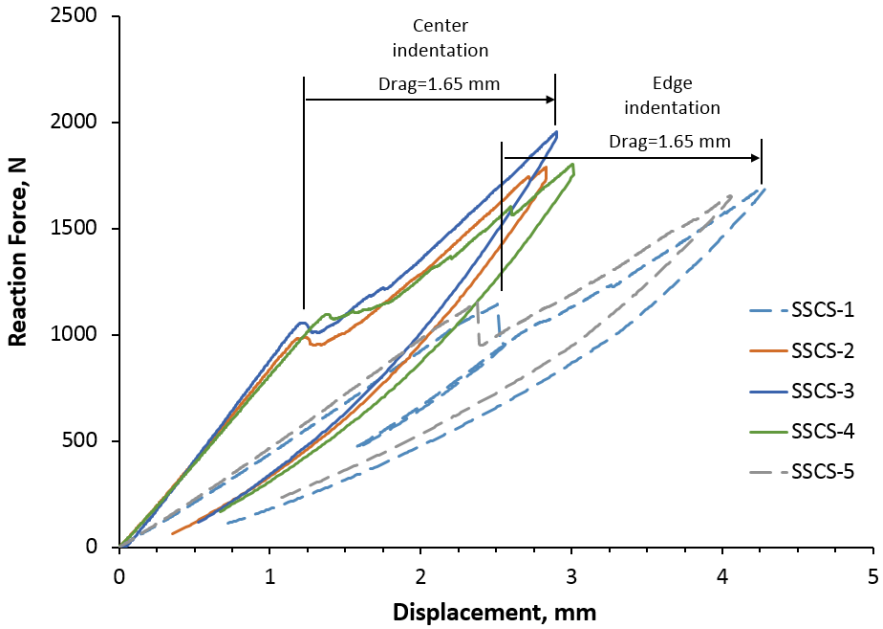

Figure 4. Force-displacement curve of indentations performed on specimens SSCS-1 to -5.

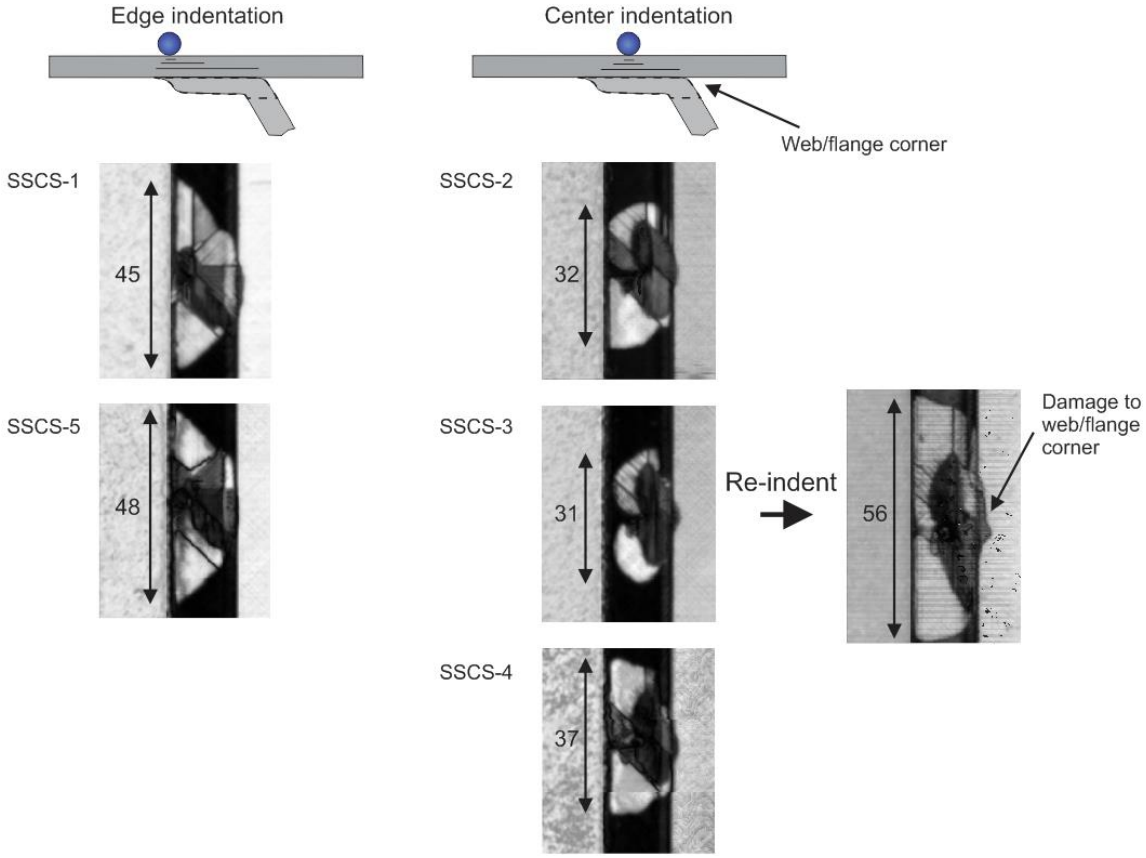

Figure 5. UT images of damage induced in specimens SSCS-1 to -5 by indenting either at the edge or at the center of the stringer flange**.**

III. Measurement of Initial Shape

Previous test campaigns conducted on SSC specimens have shown that nominally identical specimens have small imperfections and that these small differences in initial shape can result in vastly different postbuckling deformations[5]. The flatness of the skin of the specimens was measured using the VIC-3D[7] digital image correlation system. In order to capture more detail, the depth of the indentation was also measured in a coordinate measuring machine (CMM), as shown in Fig. 6. Using the laser scanning head shown in the figure, the CMM provided measurements of the surface with an accuracy of 10 μm.

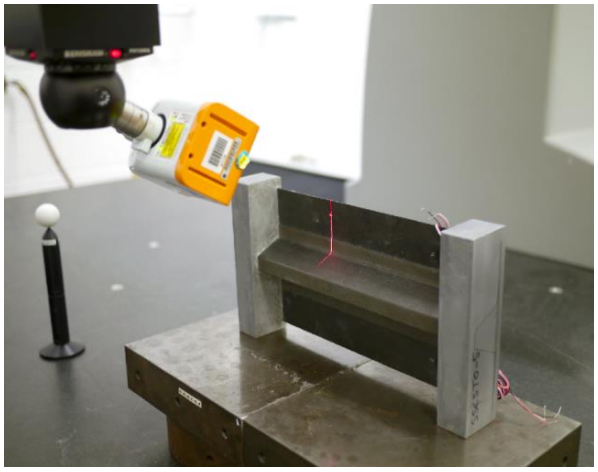

Figure 6. Laser scanning of SSC specimen with CMM.

A typical out-of-plane initial deformation of the skin measured with VIC-3D is shown in Fig. 7a. The non-flatness of the skin is mostly due to the residual thermal strains that develop from the curing process. It can be observed that the panel has a slight twist. The amplitude of the deformations is approximately 0.4 mm, which is 40% of the skin thickness.

The results from the CMM provide detail for the residual dent depth. The indentation detail of SSCS-3 shown in Fig. 7b indicates that the residual dent depth is approximately 0.1 mm.

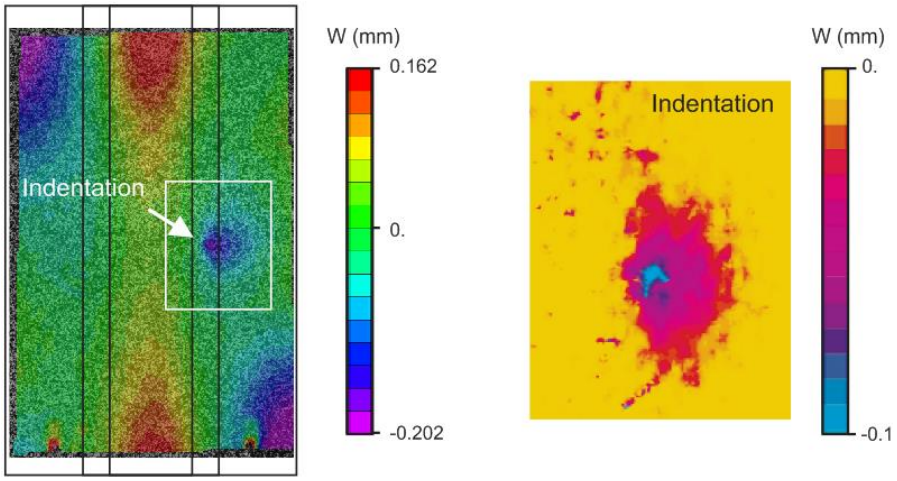

a) b)

Figure 7. Global and local out-of-plane deformation after indentation for specimen SSCS-3: a) Panel initial imperfection from VIC-3D; b) Local indentation depth measured from CMM.

IV. Testing Equipment and Instrumentation

Five SSC specimens with indentation damage were tested at the NASA Langley Research Center to study the evolution of damage under quasi-static and cyclic compression loads. A quasi-static test was performed on one of the specimens, and the other four specimens were tested in fatigue by cycling into postbuckling at 2 Hz. The tests were conducted under controlled conditions using a uniaxial test frame, and with instrumentation that allowed a precise evaluation of the postbuckling response and damage. The test frame and the instrumentation used during the tests is shown in Fig. 8. The primary instrumentation for these tests consisted of cameras for digital image correlation, an infrared camera for the passive thermal monitoring, and an in-situ UT scanner. Two back-to-back pairs of strain gauges placed on opposite faces of the skin one inch from the upper loading potting were used to align the upper platen at the start of the test.

Digital image correlation was used extensively. Specifically, two 3-dimensional digital image correlation (VIC-3D) systems[7] were used to monitor the formation and evolution of the postbuckling deformations and to measure the full-field displacements and strains on the skin and on the stringer sides of the specimen.

Passive thermal monitoring was conducted in real time during the fatigue tests using an infrared camera. Inspection by passive thermography is accomplished without the application of external heat. Instead, the rubbing of matrix cracks and delaminations induces heating that is detectable by the infrared camera. The technique is particularly useful in fatigue because it can track the position of a delamination front during fatigue cycling without stopping the test. The live information from the thermography was used to determine when to stop the fatigue tests at several stages of the damage evolution to allow detailed measurements using a non-immersion in-situ UT scanner[8]. The UT probe and the UT translation stage were mounted on the load frame and a UT inspection could be performed without removing the specimen from the load frame.

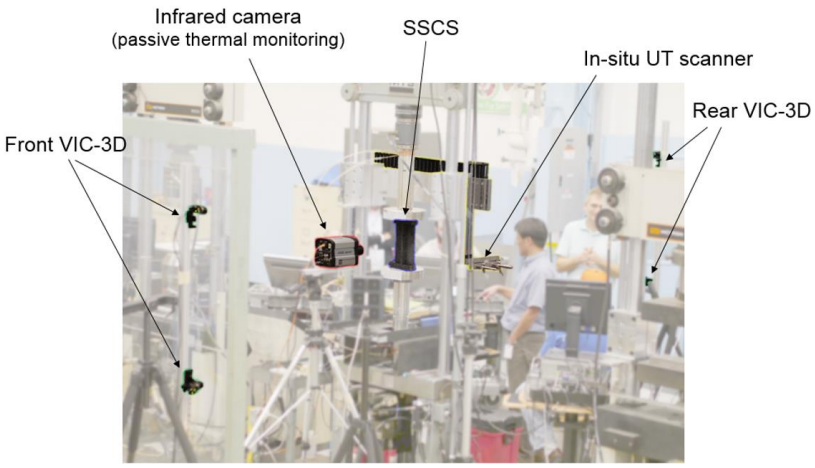

Figure 8. Test frame and instrumentation used to monitor the structural response and damage propagation. (The photo was modified to better delineate the instrumentation.)

V. Quasi-Static Test

Specimen SSCS-2 was tested statically until collapse. The collapse load was taken as reference for setting the level of the cyclic load for the fatigue tests of the four remaining specimens.

During the static compression test, the specimen initially exhibited a linear shortening. This linear response was followed by a transition into the postbuckling range that was progressive and devoid of snap-through and, as such, it was difficult to clearly identify a buckling load. The out-of-plane deformations increased gradually in the postbuckling regime and the deformation was characterized by a symmetric mode composed of three half waves along the length of the panel. The displacement field was recorded by the digital image correlation system at different load levels, and three images of the evolution of the out-of-plane displacement before the collapse are shown in Fig. 9. It can be observed that the half waves at the center of the specimen deform towards the stringer.

The collapse was preceded by an increase in the deflection at the mid-span on the side of the indentation damage, which became more pronounced and more elongated. In previous investigations, this deformation has been linked to

a transition of the postbuckling deformation under the stringer that determines the redistribution of the internal forces and leads to the delamination between the skin and the stringer flange and consequent collapse[9]. No damage was detected before the sudden collapse, which occurred at 34.5 kN.

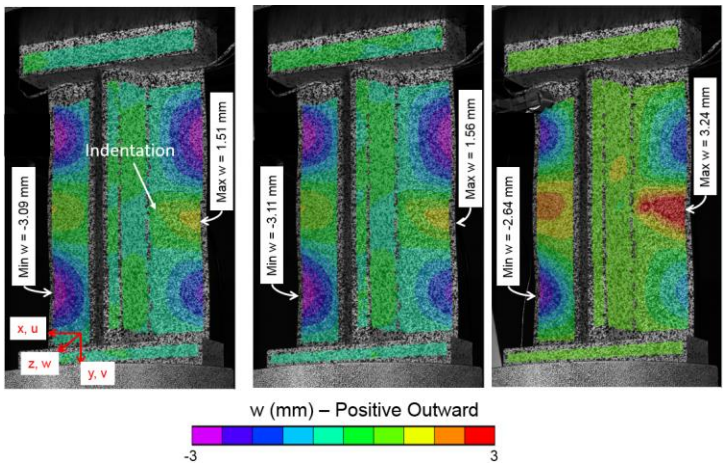

Figure 9. Out-of-plane displacement during a static test (specimen SSCS-2) taken with VIC-3D from hat side: at 28.47 kN, at 29.80 kN, and at 31.14 kN.

VI. Fatigue Tests

Four SSC specimens were tested in fatigue. These fatigue tests were conducted in stages so that UT scans of the indented area of the panel could be performed at regular intervals. Digital image correlation was used during cyclic loading to monitor the formation and evolution of the postbuckling deformations. Passive thermography and UT were used to track the evolution of damage. An image captured by the digital image correlation system on the skin side of a typical panel (SSCS-1) after 96,000 load cycles is shown in Fig. 10. When subjected to a load of 31.1 kN, the maximum out-of-plane displacement is equal to 3.42 mm in the direction opposite to the stringer, and 1.79 mm in the direction of the stringer. Specimen SSCS-1 failed at 117,506 cycles as a consequence of an unstable delamination between the skin and both stringer flanges as shown in Fig. 11.

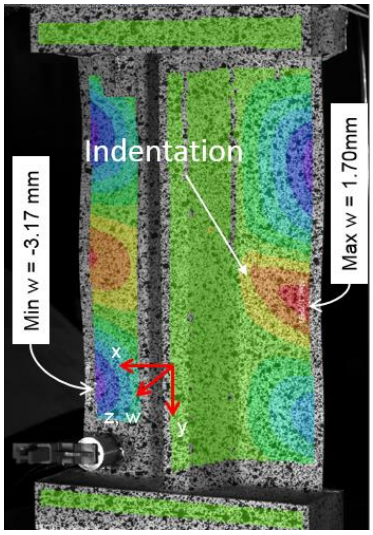

Figure 10. Deformation of specimen SSCS-1 after 96 kilocycles.

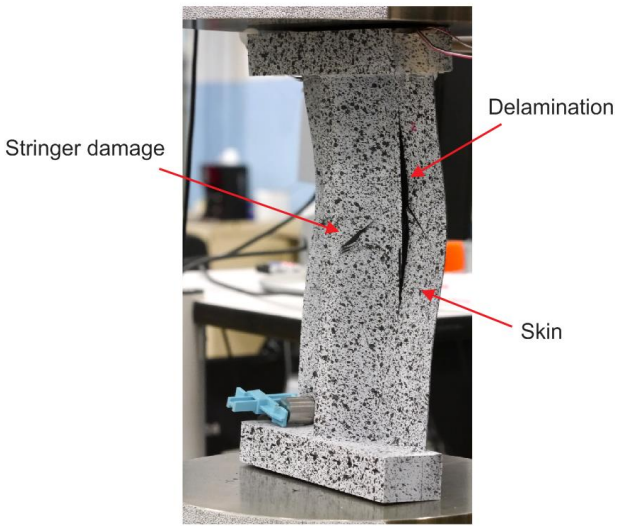

Figure 11. Deformation of specimen SSCS-1 after collapse.

The infrared image shown in Fig. 12 was captured during fatigue cycling of specimen SSCS-4. Heating (as represented by lighter regions of the image) can be seen in the image at the strain gauges and along the delamination front at the skin/stringer interface. A UT image of the damage zone is also shown for comparison. Note that the thermal image was captured from the stringer side of the specimen, while the UT scans are performed from the skin side of the specimen. Therefore, the UT image was flipped horizontally to match the infrared image.

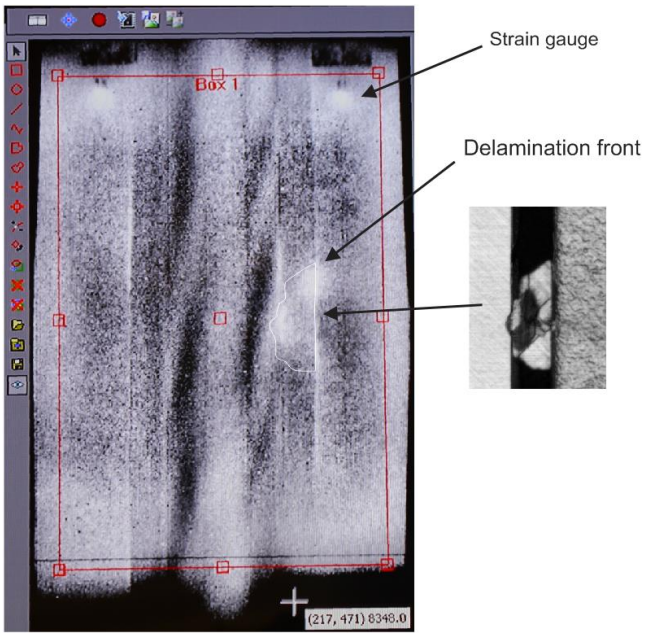

Figure 12. Infrared image captured during fatigue cycling and comparison with UT image.

The fatigue test was conducted in stages so that UT of the indented area of the panel could be performed at regular intervals. To illustrate the typical propagation of damage, a sequence of images for SSCS-4 obtained by the UT measurements immediately after indentation and at 12,000, 36,000, and 78,000 cycles are shown in Fig. 13. The images show an extension of the initial skin-stringer separation along the length of the specimen. Collapse of the specimen occurred at cycle 78,135, shortly after the last image was taken.

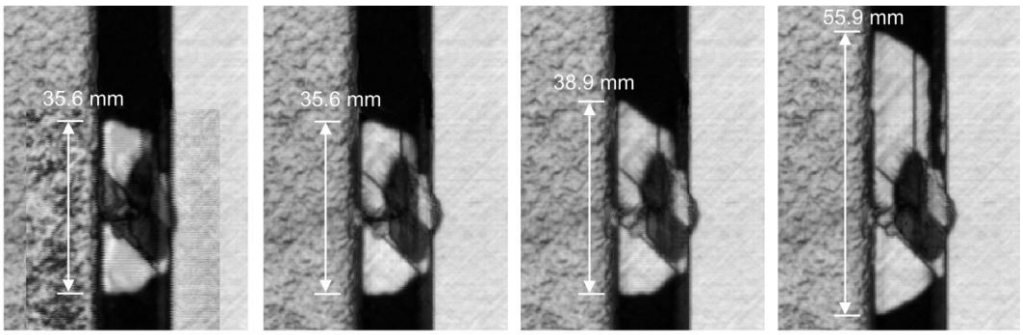

Figure 13. UT images showing the extent of the damage for specimen SSCS-4 at different cycle counts.

A study was conducted to examine the morphology of the initial indentation damage and to characterize the propagation of the damage under cyclic loading. The scan shown in Fig. 13 for 78,000 cycles was processed and colorized according to "time of flight" to characterize the location through the depth of the various delaminations. The resulting images are shown in Fig. 14, where five cross sections of the skin and stringer flange are examined. The

results indicate that the largest delamination occurs at the +45/-45 interface between the skin and the stringer. Other smaller delaminations are present in the skin at other interfaces closer to the indented surface. It was found that only two delaminations propagate during cyclic loading and that both delaminations propagate together: one interface is at the skin/stringer interface, and the other one is one-ply deep into the stringer flange, at the -45/0 interface.

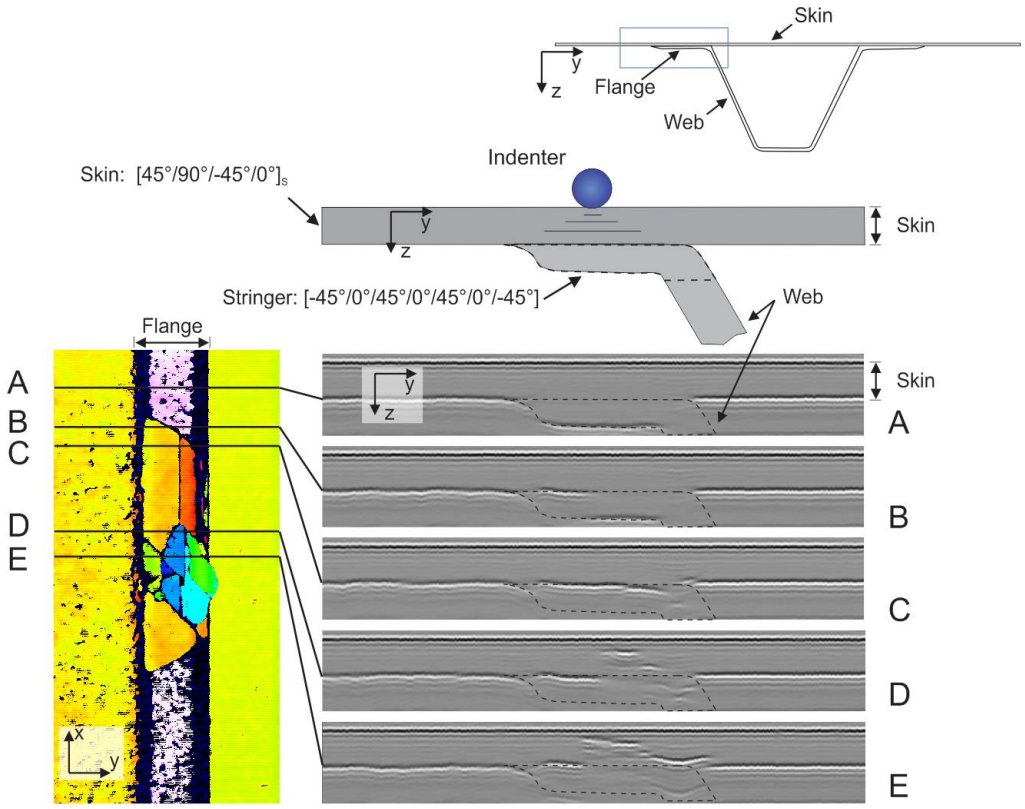

Figure 14. UT images using "time-of-flight" for location of depth of delaminations.

VII. Comparison of Fatigue Damage Propagation

The results of the present test campaign are summarized in Table 1. The specimens are grouped according to the location of the indentation: specimens SSCS-1 and -5 were indented at the edge of the flange while specimens SSCS-2, -3, and -4 were indented at the center of the flange. The initial damage length and the length of the damage at different intervals are shown. Specimen SSCS-2 was loaded quasi-statically to failure, and specimen SSCS-3 failed unexpectedly during the first loading cycle. All of the damage lengths were measured from the UT, except for the last value in the fatigue tests (shown in italic), which was estimated by using the average measured rate of propagation, as described at the end of this section.

One difficulty in performing an exploratory study in fatigue such as this one is that the cyclic loads required for a practical rate of damage propagation is unknown. In the present test campaign, an ideal rate of fatigue damage propagation would result in a collapse of the specimen in 10,000 to 100,000 cycles. However, when considering different damage sizes and other variations between specimens, the ranges of loads that cause collapse and those that cause slow fatigue damage propagation can overlap. Therefore, in several instances, the rate of damage propagation was deemed to be too low and the cyclic load was progressively increased. In the case of specimen SSCS-3, the initial cyclic load was too large and the specimen collapsed during the first loading cycle. Consequently, it becomes difficult to compare the rate of fatigue damage propagation for specimens with different damage sizes, different loads, and possibly different damage morphologies and structural responses. To enable some means of comparison, the rate of propagation was assumed to depend on a stress intensity measure, K, according to the Paris Law:

$$\frac{da}{dN} = C(K)^m = C\left(\sigma\sqrt{a}\right)^m \tag{1}$$

where σ is assumed to be the cyclic load applied to the panel, a is the length of the damage size, and N is the number of cycles. The constants C and m are determined empirically by curve-fitting the experimental results. One set of these constants is assumed for edge indentation, and another for center indentation.

Table 1. Summary of quasi-static and fatigue test results.

$C_{Edge} = 6 \times 10^{-37}$ (kN, mm) $m_{Edge} = 15$

SSCS-1 (Edge)		
Cycles X 1000	***a* mm**	**Load kN**
initial	45.0	
12	45.0	29.8
24	45.7	31.1
36	46.7	31.1
48	47.5	31.1
60	48.0	31.1
72	49.3	31.1
84	49.8	31.1
96	51.6	31.1
108	53.8	32.5
117.506	*58.3*	33.8
	K =	*258*

SSCS-5 (Edge)		
Cycles X 1000	***a* mm**	**Load kN**
initial	48.5	
12	57.2	32.5
20	59.2	32.5
30	62.0	32.5
33.623	*64.6*	32.5
	K =	*261*

$C_{Center} = 7 \times 10^{-22}$ (kN, mm) $m_{Center} = 9$

SSCS-4 (Center)		
Cycles X 1000	***a* mm**	**Load kN**
initial	36.8	
12	36.8	22.9
18		24.5
24		25.8
30		27.1
36	39.9	28.5
54	46.0	28.5
60	47.5	29.8
72	48.0	29.8
78	57.7	31.1
78.135	*57.9*	31.1
	K =	*237*

SSCS-3 (Center)		
Cycles X 1000	***a* mm**	**Load kN**
initial	56.1	27.4
	K =	*205*

SSCS-2 (Center)		
Cycles X 1000	***a* mm**	**Load kN**
initial	32.3	34.5
	K =	*196*

The results of the fatigue damage propagation are illustrated in Fig. 15, where the experimental results are represented by the symbols and the lines correspond to the damage lengths calculated with the Paris law. Two sets of parameters C and m were determined by curve fitting: one for edge indentation and a different one for center indentation. The values used are shown in Table 1. As can be observed in Fig. 15, a single set of Paris law parameters provides a good fit to both specimens with edge indentation (SSCS-1 and SSCS-5). This indicates that similar propagation laws characterize the damage growth in both specimens in spite of the differences in initial damage size and cyclic load. It is also apparent that the rate of propagation for center indentation (SSCS-4) is significantly higher than for edge indentation, perhaps because center indentation causes more damage towards the highly loaded web/flange corner than center indentation, as was discussed in Section II.

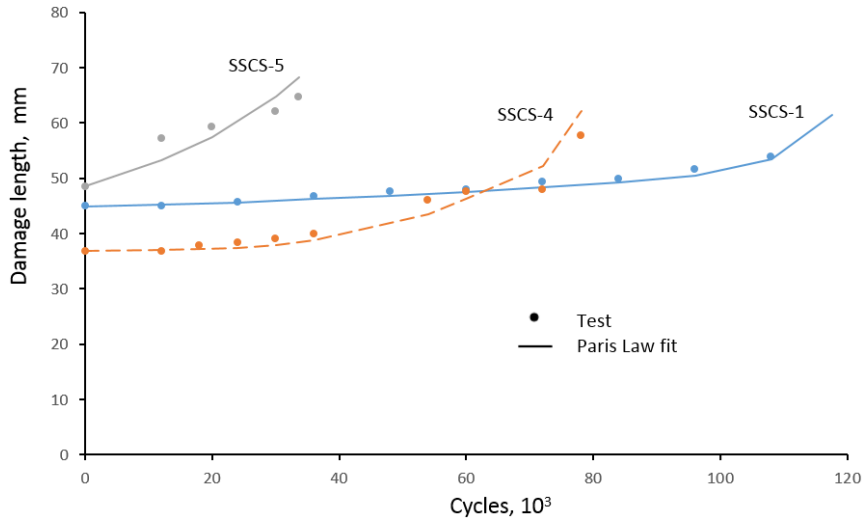

Figure 15. Damage length as a function of loading cycles for specimens SSCS-1, -4, and -5.

VIII. Comparison of Collapse Loads

For any damage size, there is a critical load that causes a collapse of the SSC specimens. It is useful to examine the effect of defect size on the collapse load. The experimental results of the present test campaign are combined with the results of three previous test campaigns in Fig. 16. The tests in phases I and II were exclusively quasi-static, while subsequent ones comprised mixes of quasi-static and fatigue tests. The damage size considered in phases I and II consists of the length of Teflon film (if present) placed between skin and stringer. In the case of fatigue tests, the defect size consists of an estimate of the damage at the moment of the collapse obtained by adding an incremental extension calculated with the Paris Law to the last measured damage length.

Following the concept used in the previous section, it may be useful to compare the results of different tests according to the stress intensity measure $K = \sigma\sqrt{a}$. Using Fig. 16, it can be observed that the edge indent specimens collapsed at approximately K = 260 kN×mm$^{0.5}$. The center indent specimens failed at $196 \le K \le 237$ kN×mm$^{0.5}$. Other specimens failed at lower values of K, which is not surprising considering, for instance, the effect of the postbuckling mode on the collapse load [2, 9]. In particular, one specimen from phase III with a 20-mm Teflon insert failed at K = 130 kN×mm$^{0.5}$, apparently due to a sudden snap-through mode change of the flange at the Teflon insert. Nevertheless, a classification of specimens according to their stress intensity measure provides a useful means to assess different aspects of the response on the damage tolerance of stiffened structures with defects.

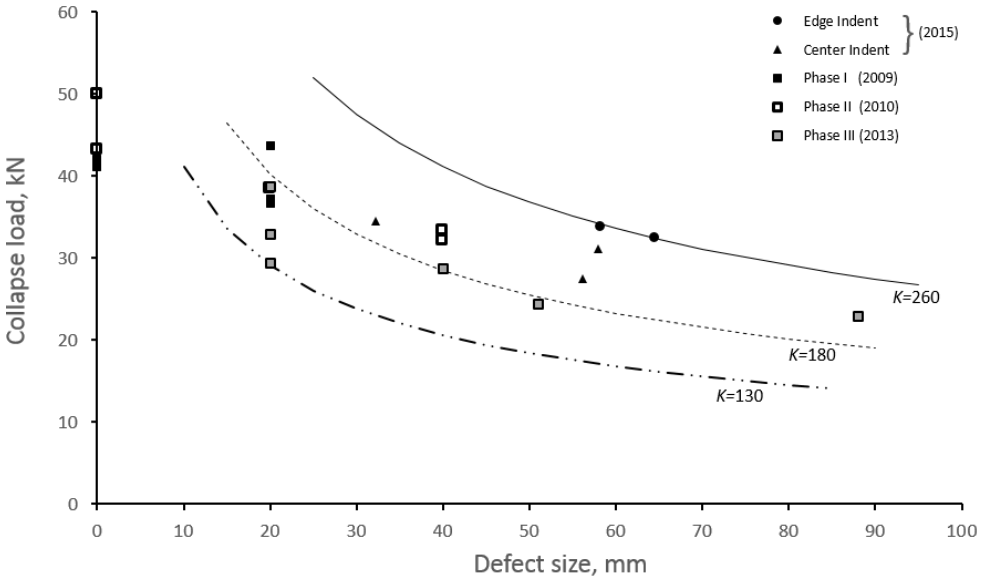

Figure 16. Effect of defect size on collapse load of SSC specimens.

IX. Summary

A series of static and fatigue tests were performed on single stringer compression specimens. Five specimens were manufactured with a co-cured hat-stringer, and an initial defect was introduced at the specimen mid-length of the stringer flange by indentation. One of the specimens was tested under quasi-static compressive loading, while the remaining four specimens were tested by cycling in postbuckling. The tests were conducted under controlled conditions and the specimens were monitored throughout the loading with multiple in-situ non-destructive evaluation (NDE) methods to obtain detailed information on deformation response characteristics and damage evolution. Three-dimensional digital image correlation was used to obtain full-field displacement measurements, and in-situ passive thermography and UT were used to track damage evolution.

Using passive thermography with an infrared camera, it was possible to monitor the growth of the initial delamination damage while the specimens were being cycled. The real-time information from the thermography was used to determine stopping points along the fatigue tests to ensure that critical stages of the damage evolution were then recorded with UT scans.

To enable a comparison between different tests, a procedure was proposed based on the concept of stress intensity measure, which is the product of the applied load and the square root of the damage size. The stress intensity measure provides the means to compare the collapse loads of specimens with different damage types and damage sizes. In addition, the stress intensity measure was applied in a Paris law to compare the damage propagation rates in specimens loaded with different cyclic loads. The empirical measures applied are not intended for use as prediction tools for damage tolerance and fatigue life because they do not account for a number of factors such as the location of the damage, the postbuckling deformation, or the shape of the damage. However, the approach does enable a comparison of different tests and the potential identification of effects that influence the fatigue lives and damage tolerance of postbuckled structures with defects.

X. Acknowledgements

The authors would like to thank the many colleagues who contributed to this effort. In particular, Dr. Kyong Chan Song for performing the indentation tests, Mr. Rufus Sykes for taking the CMM measurements, Mr. George Cowley for operating the laboratory equipment and the UT, Dr. Joe Zalameda for performing the thermography, Drs. David Dawicke and Nate Gardner for their recording and analysis of the VIC-3D data, and Dr. Cheryl Rose for providing the resources and team coordination.

XI. References

[1] Bisagni, C., Vescovini, R., and Dávila, C.G., "Single-Stringer Compression Specimen for the Assessment of Damage Tolerance of Postbuckled Structures," *Journal of Aircraft*, Vol. 48, No. 2, 2011, pp. 495-502.

[2] Bisagni, C., and Dávila, C.G., "Experimental Investigation of the Postbuckling Response and Collapse of a Single-Stringer Specimen," *Composite Structures*, Vol. 108, 2014, pp. 493-503.

[3] Bisagni, C., Dávila, C.G., Rose, C.A., and Zalameda, J.N., "Experimental Evaluation of Damage Progression in Postbuckled Single Stringer Composite Specimens," Proceedings of the 29th American Society of Composites Technical Conference La Jolla, CA, Sep 8-10, 2014.

[4] Dávila, C.G., and Bisagni, C., "Fatigue Life and Damage Tolerance of Postbuckled Composite Structures," Proceedings of the 1st Int Conf on Mechanics of Composites, Stony Brook, NY, 8-12 June 2014.

[5] Dávila, C.G., Bisagni, C., and Rose, C.A., "Effect of Buckling Modes on the Fatigue Life and Damage Tolerance of Stiffened Structures," Proceedings of the SciTech 2015, Kissimmee, FL, Jan 5-9, 2015.

[6] Dassault Systèmes, *Abaqus® 6.14 Documentation,* Simulia Corp., Providence, RI, USA, 2014.

[7] Correlated Solutions, *VIC-3D User Manual*, Columbia, SC, 2012.

[8] Johnston, P., Wright, C., Zalameda, J., and Seebo, J., "Ultrasonic Monitoring of Ply Crack and Delamination Formation in Composite Tube under Torsion Load," Proceedings of the Ultrasonics Symposium (IUS), 2010 IEEE, pp. 595-598.

[9] Vescovini, R., Dávila, C.G., and Bisagni, C., "Failure Analysis of Composite Multi-Stringer Panels Using Simplified Models," *Composites Part B: Engineering*, Vol. 45, No. 1, 2013, pp. 939-951.